AD-A228 086

REPORT DOCUMENTATION PAGE

Form Approved
OMB No. 0704-0188

1. AGENCY USE ONLY (Leave blank)	2. REPORT DATE	3. REPORT TYPE AND DATES COVERED
	18 Aug 86	Conference Presentation

4. TITLE AND SUBTITLE
Comparisons in Three-Dimensionality in the Unsteady Flows Elicited by Straight and Swept Wings

5. FUNDING NUMBERS
TA 2307-F1-38

6. AUTHOR(S)
J. Ashworth and M. Luttges

7. PERFORMING ORGANIZATION NAME(S) AND ADDRESS(ES)
F.J. Seiler Research Laboratory
USAF Academy CO 80840-6528

8. PERFORMING ORGANIZATION REPORT NUMBER
FJSRL-PR-90-0014

9. SPONSORING/MONITORING AGENCY NAME(S) AND ADDRESS(ES)

10. SPONSORING/MONITORING AGENCY REPORT NUMBER

11. SUPPLEMENTARY NOTES

12a. DISTRIBUTION/AVAILABILITY STATEMENT
Distribution Unlimited

12b. DISTRIBUTION CODE

13. ABSTRACT (Maximum 200 words)

An investigative study of the three-dimensional, unsteady flow field about a sinusoidally pitching forward swept wing, straight wing and aft swept wing was conducted. The flow field was documented using a smoke wire technique and stroboscopic photography. Photographs were taken from both side and top view perspectives at span locations from wingtip to 1.33c inboard. A comparative study between these wings is made with the smoke sheet at identical span locations for each. The unsteady flow field was produced by sinusoidally oscillating the wings about the quarter chord between angles of attack of 5 and 25 deg at reduced frequencies of 0.0, 0.6, 1.0, and 1.4. Static stall characteristics seem to directly influence the dynamic vortical structure formation, growth and traversing tendencies. The interactive effects between dynamic wingtip and leading edge vortex size and location show effects of wing sweep and reduced frequency. Multiple vortex formation during the initial phase of the pitching cycle and leading edge vortex splitting were observed. Keywords:

14. SUBJECT TERMS
flow visualization; Pitch motion; Sweptback wings; three dimensional flow; Sweptforward wings (EDC); unsteady flow

15. NUMBER OF PAGES
11

16. PRICE CODE

17. SECURITY CLASSIFICATION OF REPORT	18. SECURITY CLASSIFICATION OF THIS PAGE	19. SECURITY CLASSIFICATION OF ABSTRACT	20. LIMITATION OF ABSTRACT
UNCLASSIFIED	UNCLASSIFIED	UNCLASSIFIED	NONE

GENERAL INSTRUCTIONS FOR COMPLETING SF 298

The Report Documentation Page (RDP) is used in announcing and cataloging reports. It is important that this information be consistent with the rest of the report, particularly the cover and title page. Instructions for filling in each block of the form follow. It is important to ***stay within the lines*** to meet ***optical scanning requirements***.

Block 1. Agency Use Only *(Leave blank)*.

Block 2. Report Date. Full publication date including day, month, and year, if available (e.g. 1 Jan 88). Must cite at least the year.

Block 3. Type of Report and Dates Covered. State whether report is interim, final, etc. If applicable, enter inclusive report dates (e.g. 10 Jun 87 - 30 Jun 88).

Block 4. Title and Subtitle. A title is taken from the part of the report that provides the most meaningful and complete information. When a report is prepared in more than one volume, repeat the primary title, add volume number, and include subtitle for the specific volume. On classified documents enter the title classification in parentheses.

Block 5. Funding Numbers. To include contract and grant numbers; may include program element number(s), project number(s), task number(s), and work unit number(s). Use the following labels:

C	- Contract	PR	- Project
G	- Grant	TA	- Task
PE	- Program Element	WU	- Work Unit Accession No.

Block 6. Author(s). Name(s) of person(s) responsible for writing the report, performing the research, or credited with the content of the report. If editor or compiler, this should follow the name(s).

Block 7. Performing Organization Name(s) and Address(es). Self-explanatory.

Block 8. Performing Organization Report Number. Enter the unique alphanumeric report number(s) assigned by the organization performing the report.

Block 9. Sponsoring/Monitoring Agency Name(s) and Address(es). Self-explanatory.

Block 10. Sponsoring/Monitoring Agency Report Number. *(If known)*

Block 11. Supplementary Notes Enter information not included elsewhere such as: Prepared in cooperation with...; Trans. of...; To be published in.... When a report is revised, include a statement whether the new report supersedes or supplements the older report.

Block 12a. Distribution/Availability Statement. Denotes public availability or limitations. Cite any availability to the public. Enter additional limitations or special markings in all capitals (e.g. NOFORN, REL, ITAR).

DOD	- See DoDD 5230.24, "Distribution Statements on Technical Documents."
DOE	- See authorities.
NASA	- See Handbook NHB 2200.2.
NTIS	- Leave blank.

Block 12b. Distribution Code.

DOD	- Leave blank.
DOE	- Enter DOE distribution categories from the Standard Distribution for Unclassified Scientific and Technical Reports.
NASA	- Leave blank.
NTIS	- Leave blank.

Block 13. Abstract. Include a brief *(Maximum 200 words)* factual summary of the most significant information contained in the report.

Block 14. Subject Terms. Keywords or phrases identifying major subjects in the report.

Block 15. Number of Pages. Enter the total number of pages.

Block 16. Price Code. Enter appropriate price code *(NTIS only)*.

Blocks 17. - 19. Security Classifications. Self-explanatory. Enter U.S. Security Classification in accordance with U.S. Security Regulations (i.e., UNCLASSIFIED). If form contains classified information, stamp classification on the top and bottom of the page.

Block 20. Limitation of Abstract. This block must be completed to assign a limitation to the abstract. Enter either UL (unlimited) or SAR (same as report). An entry in this block is necessary if the abstract is to be limited. If blank, the abstract is assumed to be unlimited.

AIAA'86

AIAA-86-2280-CP
Comparisons in Three-Dimensionality in the Unsteady Flows Elicited by Straight and Swept Wings

J. Ashworth and M. Luttges, Univ. of Colorado, Boulder, CO

AIAA Atmospheric Flight Mechanics Conference

August 18-20, 1986/Williamsburg, VA

86-2280

COMPARISONS IN THREE-DIMENSIONALITY IN THE UNSTEADY FLOWS ELICITED BY STRAIGHT AND SWEPT WINGS

J. Ashworth* and M. Luttges**
Aerospace Engineering Sciences
University of Colorado, Campus Box 429
Boulder, Colorado 80309

Abstract

An investigative study of the three-dimensional, unsteady flow field about a sinusoidally pitching forward swept wing, straight wing and aft swept wing was conducted. The flow field behavior was documented using a smoke wire technique and stroboscopic photography for flow visualization. Photographs were taken from both side and top view perspectives to visualize flow patterns at span locations from wingtip to 1.33c inboard. A comparative study between these wings is made by introducing the smoke sheet at identical span locations (percent chord length) for each wing. The unsteady flow field was produced by sinusoidally oscillating the wings about the quarter chord between α = 5° and 25° at K = 0.0, 0.6, 1.0 and 1.4. Static stall characteristics for each wing were analyzed and seem to directly influence the dynamic vortical structure formation, growth and traversing tendencies. The interactive effects between dynamic wingtip and leading edge vortices are noted across the span of each wing. The wingtip and leading edge vortex size and location show effects of wing sweep and K value. For some test conditions, multiple vortex formation during the initial phase of the pitching cycle and leading edge vortex splitting were observed.

*Graduate Research Assistant, Department of Aerospace Engineering Sciences, Member AIAA

**Professor, Department of Aerospace Engineering Sciences, Member AIAA

Nomenclature

ASW	aft swept wing
c	wing chord length measured parallel to the freestream tunnel velocity
FSW	forward swept wing
K	nondimensional reduced frequency parameter, $K = \omega c/2V_\infty$
S	nondimensional spanwise distance from wingtip
STW	straight wing
SZ	nondimensional leading edge vortex size, measured from wing surface to top of vortical structure
V_∞	freestream tunnel velocity
α	instantaneous wing angle of attack (Deg.)
β	spanwise deflection angle at the wing tip (Deg.)
Λ	wing sweep angle = 30° (forward and aft)
ϕ	nondimensional oscillation phase angle (% cycle beginning at α_{max})
ω	rotational frequency in radians/sec.

Introduction

High performance aircraft envisioned for future development must possess operational capabilities in expanded flight regimes extending from very high to very low speed flight. Operations across such regimes must utilize swept wing technology to be efficient and high lift aerodynamics to be effective[1,2]. The extent to which swept wing configurations may affect such controlled stall will determine the applicability of unsteady flows to future aircraft performance.

Previous studies[3-6], done with two-dimensional airfoils, have indicated that lift enhancement is possible using unsteady flows generated in controlled fashion. More recently, unsteady flows about straight wings[7,8], delta wings[9], and swept wings[10,11,12] have been studied for sinusoidal pitching motions. These three-dimensional studies have been bolstered by straight wing studies done for large angle of attack motions as well as for linear accelerations at a variety of angles of attack[13,14]. In all of the above studies, the detailed impact of comparative sweep angles remains unclear. Yet, the existing research suggests that the sweep angle has a profound effect on both the genesis and development of unsteady flows elicited by various pitching motions.

The present study focuses on wing sweep effects. Studies were done with three test wings that varied only in sweep angle: forward, straight and aft swept. The wing tip configurations were matched to simple flat tips. Identical test conditions were used both in the static and pitching evaluations. Using multiple phase-locked photographic exposures, the evolving flow fields were examined both in side view and from above with smoke delivered to a variety of span locations. The resulting analysis revealed sweep

angle variations in the initiation of vortices and in the type of vortical structures produced on the top surface of each wing. The relation of these structures to the forcing conditions that produced them was evaluated.

Methods

All studies were conducted in the 40.5 x 40.5 cm flow visualization wind tunnel at the University of Colorado. The Reynolds numbers for all tests were 30,000 or 40,000. The smoke wire technique previously reported by Adler and Luttges[7] was used to deliver dense smoke to any desired span location on the test wing surfaces. Smoke illumination was provided by a short duration (7 μ sec) focused stroboscopic flash unit positioned about the tunnel to maximize illumination and minimize spurious reflections or diffuse lighting. Flow visualization photographs were prepared using 35mm film developed at ASA 800-1000. The dynamic tests of the three wings were done using a mean angle of attack of 15° and an oscillation amplitude of 10°. Each wing was rotated about the 0.25 chord location by a small (1/6 hp) D.C. motor. The reduced frequency values were varied from 0.0, 0.6, 1.0 to 1.4K. Photographs were prepared for discrete span locations varying from the wingtip, 0.17, 0.33, 0.5, 0.67, 1.0 to 1.33c inboard. To match the dynamic test conditions, flow visualizations were prepared for the wings at a variety of angles of attack and at different span locations for static test conditions. Although aluminum NACA 0015 stock with a 15.2 cm chord was used for all test wings, the effective chord of the straight wing was 15.2 cm compared to 17.6 cm for the swept wings.

In order to determine the interactive dependencies between wing test dynamics and the time dependencies of flow structure initiation, the whole sinusoidal oscillation period was examined by flow visualization. Photo documentation was done, however, only for those periods in the wing motion that were essential to understanding flow initiation and development. Vortex initiation point, vortex size, spatial time dependent positions, shear layer development and boundary layer growth were measured. These measurements were completed from both side and overhead views. The results were compared for different wing sweep angles at various span locations.

Results

Static Comparisons

Comparisons between straight and swept wings reveal very different spanwise flow separation characteristics. To visualize these differences and provide a basis for dynamic comparisons, the smoke sheet was introduced into the flow field to intercept each of the wings at three spanwise locations; wingtip, 0.67c and 1.33c. For each spanwise observation, angles of attack were varied from 3° to 27°. The flow field was photographed from sideview (tip to root) and from above.

A sideview comparison at $\alpha=15°$ is shown in Fig. 1. The left column for the FSW indicates a strong helical wingtip vortical structure at S = 0.00c, while the beginning of a separation layer is evident at S = 0.67c, and a fully separated flow is present at S = 1.33c. The STW, center column, also indicates a wingtip vortex at the tip, however, both inboard locations are fully stalled. The right column, ASW, shows stall characteristics along the span that are the reverse of those shown by the FSW. The wingtip flow for the ASW does not roll into the clear helical wingtip pattern shown by other wings. On the ASW, the tip flow seems to be influenced by a stalled condition very near this tip location. Inboard spanwise visualizations indicate a fully separated flow region at S = 0.67c and a less aggravated stall pattern at S = 1.33c. These static stall characteristics are consistent with previous studies[1,2,11] and theory[15].

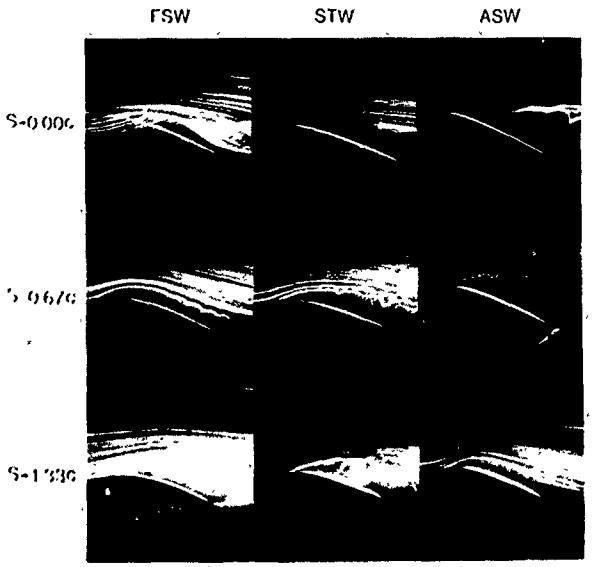

Fig. 1 Sideview static stall comparison $\alpha=15°$.

To quantify the relative apparent strength of the wingtip vortex for each wing, a spanwise flow angle β was measured at the tip of each wing. Fig. 2, graphically depicts the measurement of this angle. Top view photographs show the initial chordwise crossing of the smoke sheet from the pressure to the suction side of the wing. A line tangent to the flow is drawn at the point where the smoke initially crosses the plane of the wingtip. The angle β is measured from this tangent line to the plane of the wingtip.

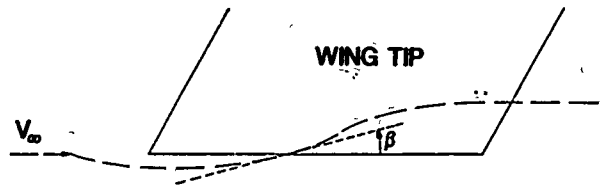

Fig. 2 Tip deflection angle, β .

Topview photographs of the wingtip flow are shown in Fig. 3, for the three wing configurations at α = 27°. The helical wingtip flow is visualized by the bending of the smoke sheet about the tip. Different comparative magnitudes of β can be seen with maximum β values observed for the FSW. The chordwise location of the flow passing around the wingtip varies not only for each wing at α =27° but also for the same wing when visualized at different phases in the oscillation cycle.

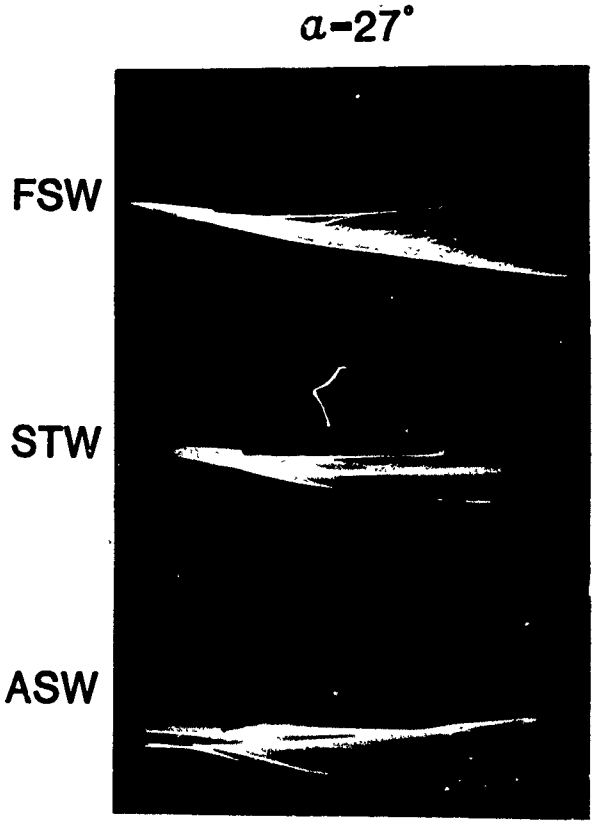

Fig. 3 Topview static β comparison, α = 27°.

The spanwise flow deflection at the wingtip, β ,is plotted for the three wing configurations over an α range from 3° to 27° (Fig. 4). Specific patterns of β variations occur throughout α increments for each wing. For the FSW, β increases with increased α throughout the α range. The β values of the STW, however, initially increase with increasing α then remain constant between α = 9° to 15° (near static stall angle for this airfoil section) and finally decrease with increased α . The β values for the ASW increase with α up to α = 9° then steadily decrease as α is increased. The highest magnitude of the ASW β value does not reach the level of values recorded for either the FSW or STW.

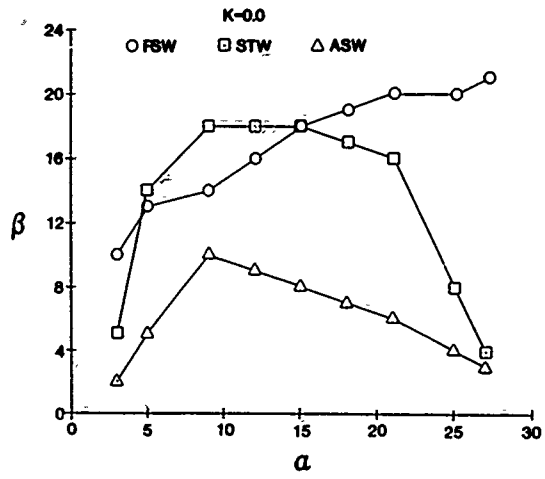

Fig. 4 Static β comparison.

Dynamic Tests: Wingtip Flow

When the test wings were forced into sinusoidal pitching motions, the flow field about the wingtip remained dominated by the strong wingtip vortex. A comparison of the observed inboard deflection angles of tip flows for each wing is provided in Fig. 5, where K = 1.0. In all cases, when the wings pitch upward, β values increase to a maximum level near maximum angles of attack. The β values then persist above those for static α tests until the lowest angles of attack are attained. Rapid decreases in β values are observed when the wing pitches to minimum angles of attack. Minimum β values occur in all tests at approximately α = 12° during the upstroke of the pitching cycles. The hysteresis loop of dynamic data collected for the FSW is centered about the static α measurements. In contrast, both average STW and ASW hysteresis loops show β values that are consistently above those measured in comparable α , non-pitching cases. The highest average magnitude of β was recorded for the STW. The pitching ASW showed a hysteresis loop for β values that contained the widest excursions between those occurring during the downstroke and those of the upstroke of the pitching cycle. An increase in K value during all wingtip observations produced downstroke and upstroke β values that formed more closed hysteresis loops.

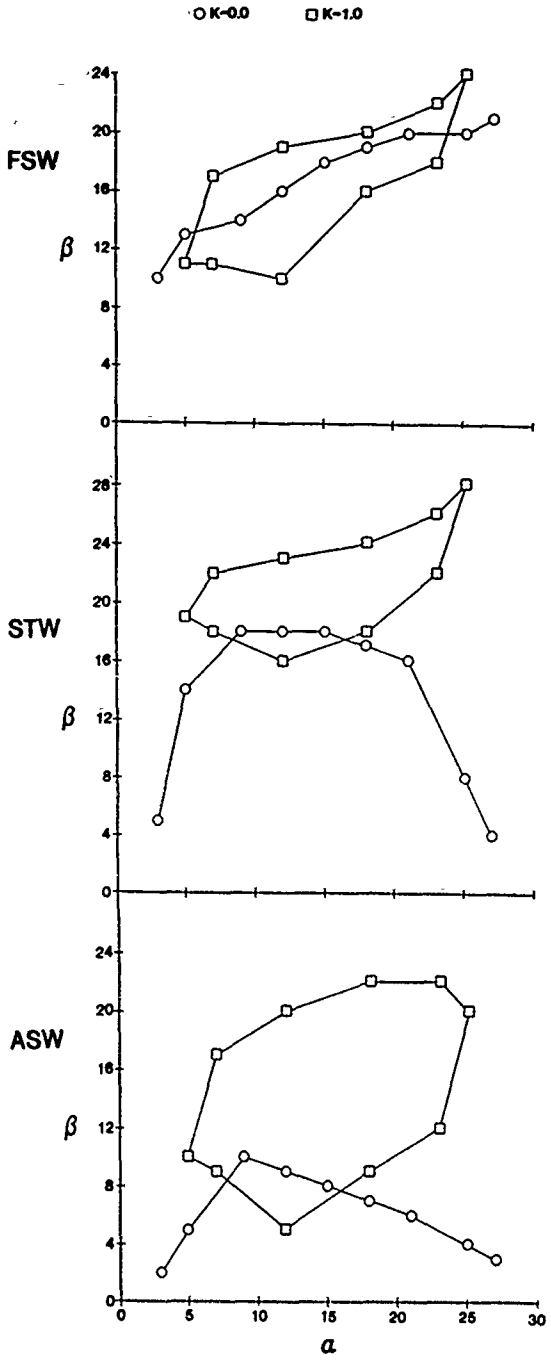

Fig. 5 Dynamic to static β comparisons, K = 0.0 and K = 1.0.

Dynamic Tests: Leading Edge Vortex On the Wing Surface

Direct comparisons between the different wing configurations in the initiation of leading edge vortices were achieved using visualizations based on smoke sheets introduced at span locations of S = 0.00, 0.17, 0.33, 0.50, 0.67, 1.00 and 1.33c. Ten sideview, multiple exposure photographs were prepared representing equal time increments throughout the oscillation cycles for K = 0.6, 1.0 and 1.4. Where and when a leading edge vortex was produced depended both on wing configuration and spanwise proximity to the wingtip. A comparative analysis of apparent leading edge vortex size and chord position over the wing top surface was done for all dynamic test conditions.

A comparison of the flow fields produced about each wing configuration at S = 0.67c and K = 1.0 is depicted in Fig. 6, for one complete oscillation cycle. Each photographic series shows the formation of a vortex near the leading edge as the wings approach maximum angle of attack, α = 25° (phase angle ϕ = 0.0). Despite the similarity in vortex initiation, each wing configuration differs in leading edge vortex growth, development and traversing characteristics. These differences can be seen in side-by-side comparisons in Fig. 6.

The FSW, left column, shows the formation of a small leading edge vortex as well as a second vortex, near midchord, during the early portions of the pitching cycle. The leading edge vortex remains stationary near the leading edge showing little growth while the second vortex both traverses toward the wing trailing edge and appears to grow in size. Coincident with the second vortex shedding from the trailing edge, ϕ = 0.4, the leading edge vortex can no longer be visually resolved in an apparent shear layer which covers the entire top surface. No leading edge vortical structure is evident until the wing again approaches the maximum angle of attack in the next oscillation cycle. The STW, center column, also forms both a leading edge vortex and second downstream vortex structure at maximum α. The leading edge vortical structure grows and seems to become turbulent when the second vortex is shed, ϕ = 0.4. The ASW, right column, initially forms a much larger definite leading edge structure. This structure continues to increase in size as it convects over the wing surface.

The relations between apparent leading edge vortex positions along the top surface of each wing are summarized in Fig. 7, for different phases of the oscillation cycle. These planform diagrams depict the leading edge vortex position across the wingspan for one half of a pitching cycle, ϕ = 0.0 to 0.5, using K = 1.0. A shear layer was present on the aft portion of the FSW. It extended from the wingtip to a span location of nearly S = 1.00c inboard. This layer appeared to prevent the formation of a discernible leading edge vortex near the wingtip. It also appeared to inhibit the downstream convection of the leading edge vortex even at span locations more inboard than S = 1.0c. Near midspan, this shear layer engulfed the leading edge vortex when the second vortex (formed near midchord) was shed from the trailing edge. The STW produced more conventional vortex growth

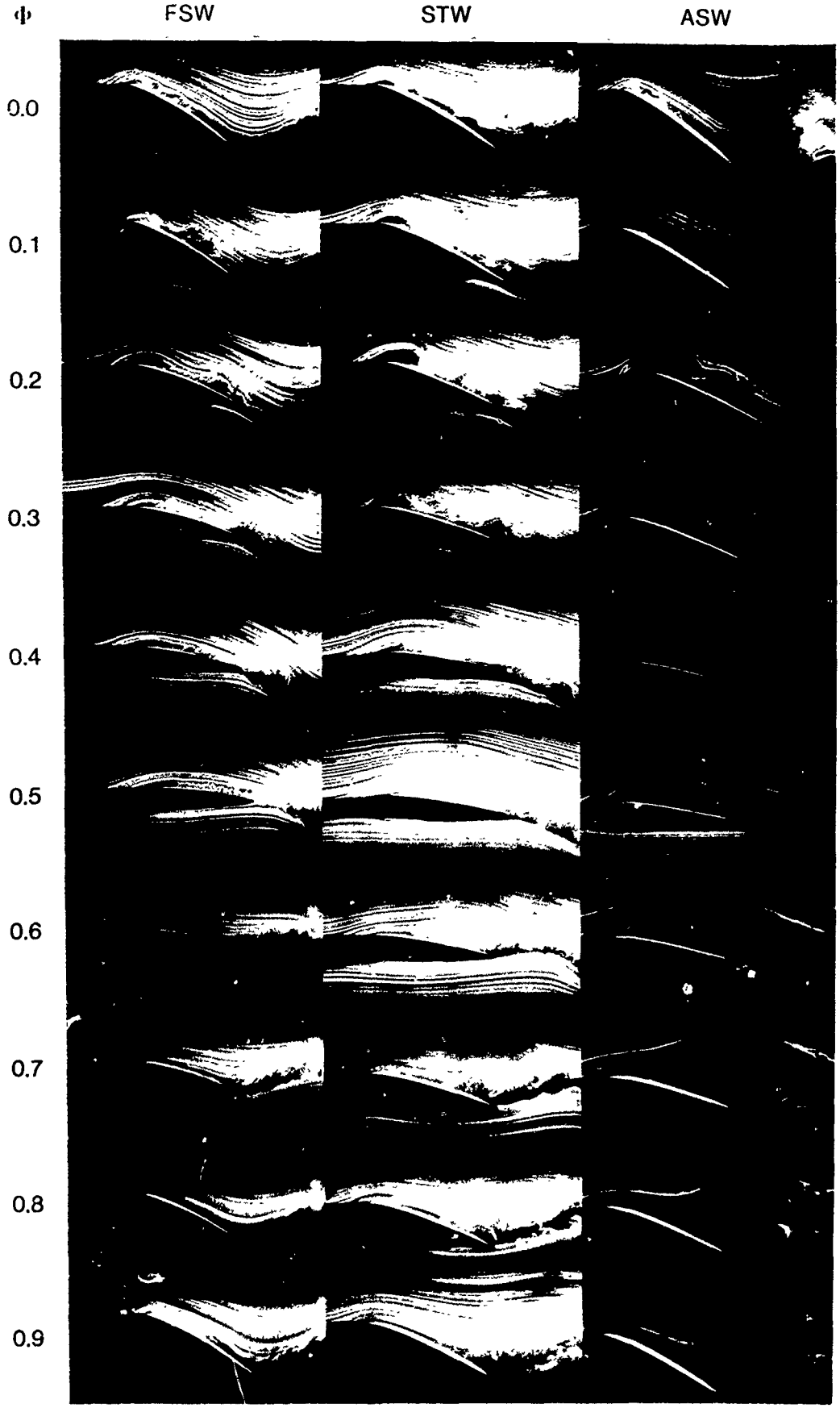

Fig. 6 Photographs of one pitching cycle, S = 0.67c, K = 1.0, ϕ = 0.0: α = 25°, ϕ = 0.5: α = 5°.

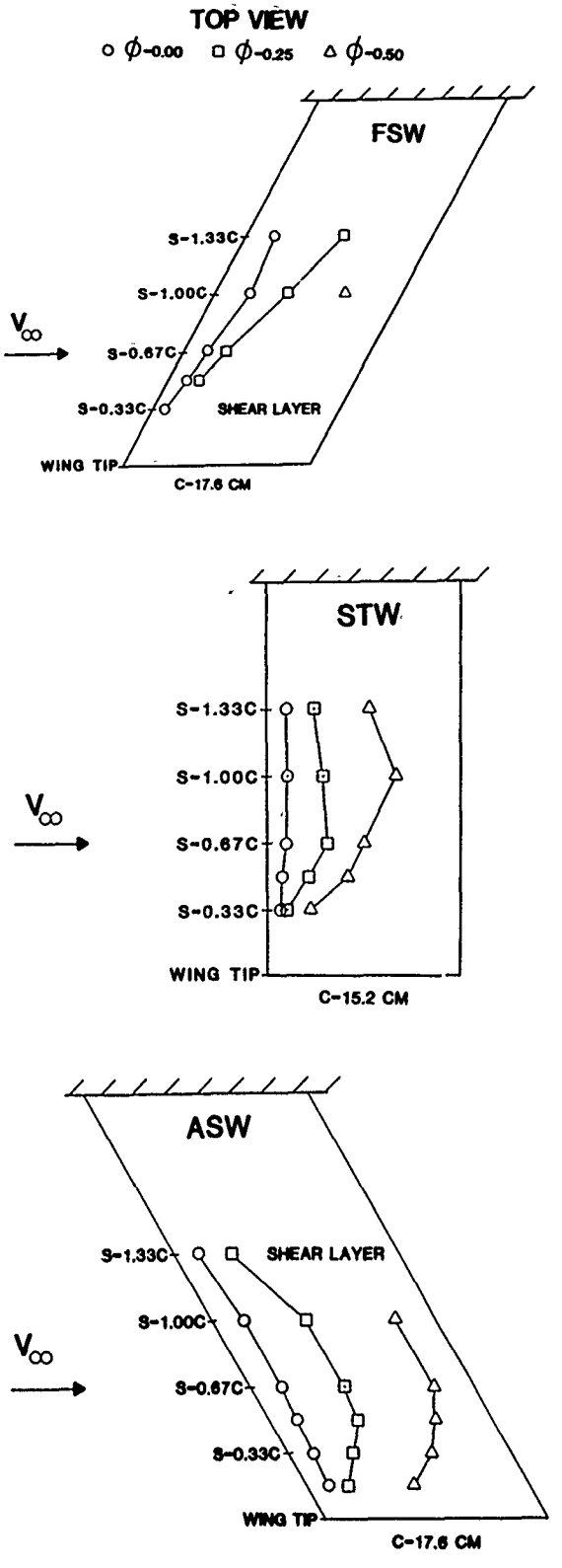

Fig. 7 Planform of leading edge vortex position, K = 1.0, ϕ = 0.0: α = 25°, ϕ = 0.5: α = 5°.

and convection characteristics. The fastest convection of the leading edge vortex occurred at S = 1.0c. A distinct leading edge vortex was present on the ASW even at a location, S = 0.17c, very near the wingtip. Quite proximal to the tip, the wingtip vortex seemed to cause the leading edge vortex to become turbulent and to move upward, away from the top surface of the wing. A shear layer apparently was present near the ASW root position, S = 1.33c, resembling that observed near the wingtip in the FSW tests. For all wing configurations, the convection velocities of the leading edge vortex across the upper wing surface were slower near the wingtip than the more inboard locations investigated.

Leading edge vortex size was dependent on span location and wing configuration. Plots of vortex size are shown in Fig. 8, for K = 1.0. The leading edge vortex size was, on an average, consistantly smaller for the FSW than for the other two wings. A shear layer dominated the FSW for S = 0.33c and 0.67c. Farther inboard, S = 1.0c and 1.33c, the leading edge vortex is well developed but remains small in size compared to vortices of the STW and ASW.

The largest leading edge vortical structures were observed for the STW at S = 1.0c. The leading edge vortex structures for the STW were small near the wingtip, S = 0.33c and S = 0.67c, and were somewhat larger near the root test position, S = 1.33c.

The ASW leading edge vortex size varies most for different spanwise test locations. Near the wingtip, S = 0.33c and S = 0.67c, the leading edge structures for the ASW developed to a larger relative size than observed using the other two wings. As spanwise test location was increased to more inboard sites, an apparent shear layer began to form and dominate the flow field as the second vortex was shed off the trailing edge.

Altered K values of 0.6, 1.0 and 1.4 caused variations in leading edge vortex size and chord location for each wing tested. The variations produced by different K values, however, were similar to those reported earlier[7,11]. No qualitative changes occurred and the flow fields were characteristic of the sweep effects noted above. Thus, the higher K values yielded more cohesive leading edge structures. For the STW, the structures appeared energetic enough to cause splitting of the initial leading edge vortex structure into separate vortices.

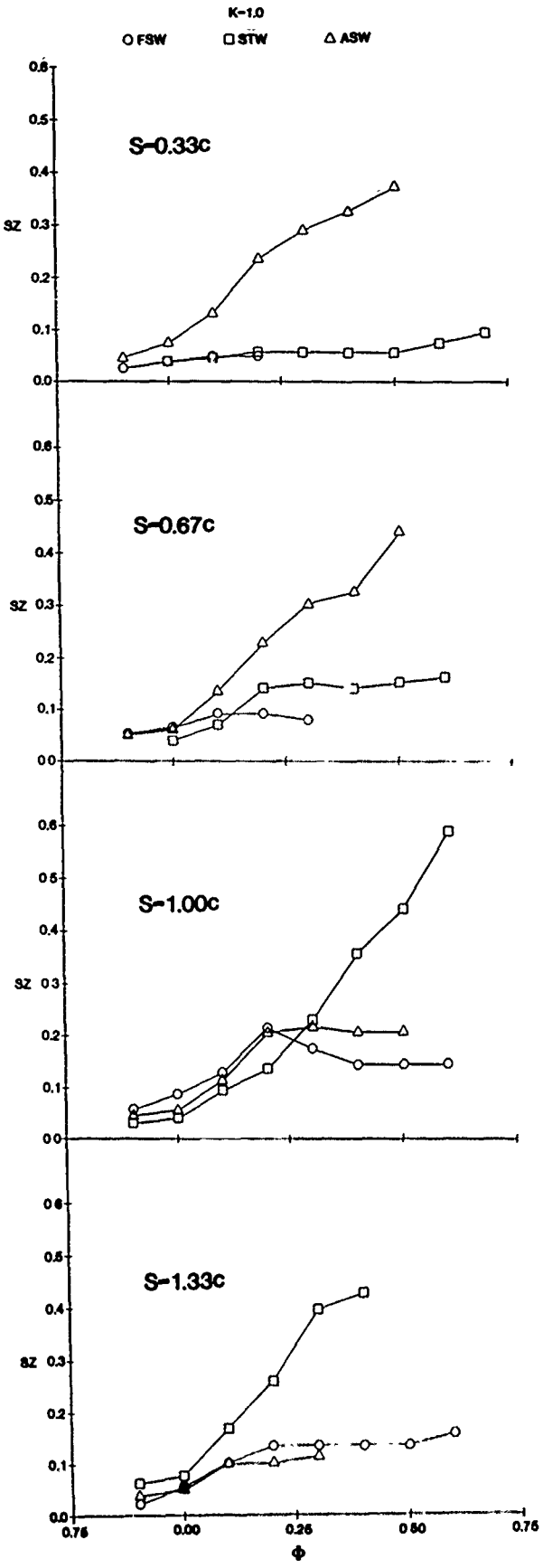

Fig. 8 Leading edge vortex size, K = 1.0, S = 0.33c to S = 1.33c.

Other Observed Phenomenon

On the surface of the STW using K = 1.4, the leading edge vortex was observed to split into two separate vortical structures. One complete pitching cycle is displayed in Fig. 9, for a span location of S = 0.67c. At or near the top of the pitching cycle (A, where $\alpha = 25°$), multiple vortex structures can be seen forming along the top wing surface. As the pitching cycle carries the wing downward (B,C, & D), primary and secondary vortices are clearly formed and are beginning to convect toward the trailing edge of the wing. The primary vortex then appears to split into two components (E & F): (1) a smaller, upstream leading edge vortex, and (2) a larger, downstream vortex comprised of a considerable amount of turbulence. Each structure then convects and is shed in tandem from the trailing edge (G through J).

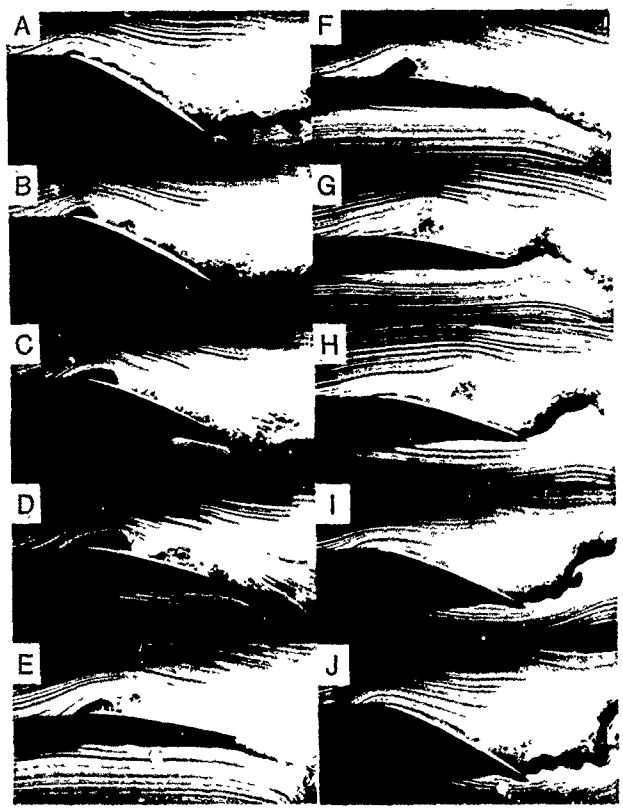

Fig. 9 Leading edge vortex splitting over one pitching cycle, STW, S = 0.67c, K = 1.4.

Additional details of the splitting of the leading edge vortex across the wingspan are depicted in Fig. 10. Near $\phi = 0.0$, a distinct vortex is seen to form nearly parallel to the leading edge at all span locations inboard of the wingtip. At approximately $\phi = 0.25$ on the downward part of the pitching cycle, the primary vortex has split into two vortical structures, each with separate positions on the wing surface. Halfway through the

pitching cycle, ϕ = 0.5, the distance between the two vortex centers has increased and at ϕ = 0.75 the more turbulent vortex core has shed from the trailing edge. The primary leading edge vortex continues to convect toward the trailing edge. This splitting phenomenon also was observed for the ASW but the magnitudes of the primary leading edge vortices were very small. No splitting was observed for the FSW.

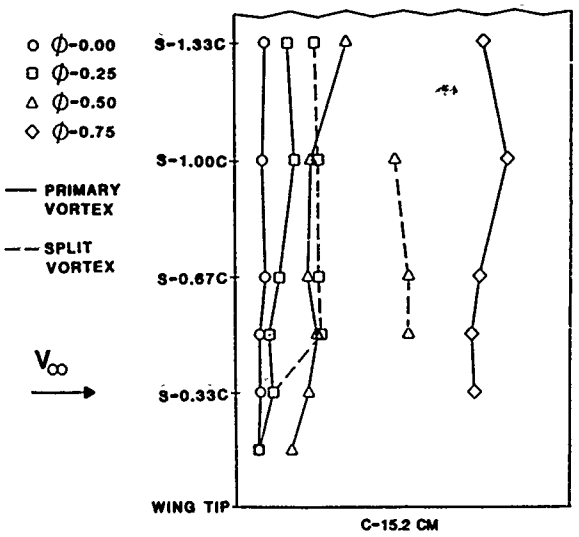

Fig. 10 Planform of leading edge vortex splitting and traversing, STW, K = 1.4.

Discussion

When tested under identical static and dynamic conditions, the FSW, STW and ASW yield different flow separation characteristics. Major differences between these wings appear to derive from spatial variations in the static separation and from the spatial and temporal distribution of vorticity related to forced dynamic separation conditions. In static testing, the FSW first began to indicate flow separation characteristics near the wing root as angle of attack was increased. Similar separation characteristics developed near midspan locations only as higher α values were tested. This stall characteristic was shared by the tip flow deflection angle, β, which increased steadily with increasing α signifying little stall influence at the wingtip.

The STW shows stall across most of the wingspan at α values near 12°. Above this α, the β values drop off reflecting the influence of the stalled wing region inboard.

Separation characteristics were first noted on the ASW near the wingtip as α was increased. This is reflected as steadily decreasing β values as α is increased even more and as inboard stall becomes more fully developed.

These differences in static tests appear to provide the basis for most of the differences between the wings when subjected to dynamic pitching tests. A spanwise comparison of static and dynamic results indicates a direct relation between static stall magnitude and dynamic leading edge vortex size. The FSW stalls first near the wing root and this region shows the largest leading edge vortical structures during dynamic testing. The ASW, however, stalls more readily near the wingtip. Accordingly, this area develops the largest dynamic vortex. Except for the FSW, the average dynamic β values are consistently higher than the static α counterparts. All β hysteresis loops for K = 1.0 are at minimum values at instantaneous α = 12° during the upstroke of the pitching cycle. This point in the pitching cycle coincides with the shedding of the inboard leading edge vortices into the wake. At = 12°, no major leading edge vortical structures are evident on the top surface of the wing.

The wing sweep effects are most dramatically illustrated in the spatial distribution of the leading edge vortices. As the wing sweep angle progresses from forward to aft, the leading edge vortex dynamics are clearly less dominated by the wingtip flow effects. A strong leading edge structure is observed on the ASW at span locations very near the wingtip, but in the FSW tests these vortices are spatially supported only at quite inboard span locations. These vortex initiation site differences suggest that as the wing sweep increases aft, more vorticity may be generated on the wing top surface to resist the wingtip effect. The resulting vortices reflect differences both in the sites of vortex formation and in the apparent development of the vortices.

A comparison of spanwise centers of leading edge vortex cores can also be made to those observed for linearly accelerated flow tests[13]. The spanwise vortical structures form nearly parallel to the leading edge of each wing and convect in a pattern dependent on wing geometry. Those patterns are reminiscent of those in the stained boundary layer flows in accelerated flow tests. Under these conditions, the structures originate at the leading edge of the wing tip and extend across the span of the wing.

Of particular note in the characteristic formation and convection of the leading edge vortex are the dynamic consequences related to the second vortex shedding from the wing trailing edge. In numerous test cases, when the second vortex that formed near midchord sheds from the top surface, the leading edge vortex decreases in apparent size and a dominant shear layer develops on the top wing surface. This shear layer sometimes completely engulfs the leading edge structure. The loss of focused vorticity from the wing top surface that apparently

occurs with second vortex shedding, causes the remaining leading edge structure to dissipate into the strengthened distributed shear layer. In cases where larger, more developed leading edge vortices exist, the shear layer is not evident and the leading edge structure successfully traverses the whole wing chord. These latter characteristics are much like those demonstrated in two-dimensional airfoil tests[6].

An increase in K seems to deposit more or more focused vorticity to the top surface of the wing. At K = 1.4, not only leading edge vortices but also second and sometimes multiple vortices are formed on the top surface at the beginning of the pitching cycle. When multiple structures are formed, the leading edge and second vortex structures often coalesce early in the downstroke of the pitching cycle. When only two structures exist on the surface, a splitting occurs: the leading edge vortex splits into a smaller leading edge structure and a larger, more turbulent downstream vortex. The three distinct vortices then separately convect over the wing chord and shed from the trailing edge.

Conclusions

The comparative spanwise observations of the three wings indicate that sweep angles can have a major influence on the static stall characteristics of the wings and in turn, the generation and development of unsteady separated flows on pitching wings. The spanwise static stall characteristics for each wing configuration enhance predictability of dynamic responses. At span locations where static stall is known to be fully developed, the leading edge vortex structure is seen to be larger and more resistant to other flow influences. This is indicated by inboard flow on the FSW, most spanwise locations on the STW and by regions adjacent to the wingtip on the ASW. At span positions where static stall occurs only at very high α, near the wingtip for the FSW and far inboard for the ASW, the dynamic leading edge vortex development is suppressed. Also, these leading edge structures are likely to be lost to the distributed vorticity of a shear layer.

Dynamic responses to sweep angles show characteristics that depend on both wing configuration and wing span location. In some cases, the leading edge vortex growth and convection were reminiscent of airfoil tests[3-6] or wing tests[7,8] where results were collected at sites distal to the wingtip. Other conditions show additional wingtip and leading edge vortex interactive effects[9-12].

At the wingtip for each wing, the dynamic β hysteresis loops show direct relationships to the presence or absence of a leading edge vortex on the wing surface. When a fully developed leading edge vortex is formed on the inboard surface, the dynamic β is highest and goes to a minimum when the leading edge structure has shed or is no longer discernible on the top surface. The overall higher average β hysteresis loops verses the static β values indicate that dynamic pitching may enhance lift production more for the STW and ASW than for a FSW which already demonstrates favorable high angle of attack lift characteristics.

The effect of wing sweep at different span locations can also be quantified by leading edge vortex size as well as vortex position on the wing surface. For the FSW, as span positions closer to the wingtip are examined, the leading edge vortex decreases in size and resists convection. This characteristic is observed, to a lesser extent, for the STW, as has been documented previously[10]. The ASW, however, shows a tendency toward larger leading edge vortical structures near the wingtip and smaller leading edge vortices far away from the wingtip. These overall characteristics, as noted earlier, seem related to static stall areas. The FSW leading edge vortex development and convection are influenced farther inboard along the wing span by the wingtip effect than STW and ASW counterparts. The leading edge vortex convection for the FSW is surpressed and even eliminated by a shear layer for span locations near S = 1.0c. This surpression is observed for the STW for a distance of only S = 0.33c inboard and no effect is seen for the ASW. The larger leading edge structures formed near the wingtip on the ASW seem to be able to resist the wingtip effect and to convect in a manner more like that observed on airfoils.

Increasing K causes what appears to be more energetic vortex development on the top surface. This leads to the formation of multiple vortices during early portions of the downstroke of the pitching cycle. A splitting of the highly energetic leading edge vortex occurs midway through the downward pitching cycle. A smaller, primary leading edge vortex remains near the leading edge while a larger, seemingly more turbulent vortex splits from the downstream side of the flow structure. These distinct structures then separately traverse the wing and shed from the trailing edge. This splitting may indicate a high level of vorticity present on the top wing surface capable of supporting three distinct vortices. Or, the available vorticity may be quite differently distributed on the wing surface. In any event, higher K values for the STW may imply more vorticity and possibly greater lift enhancement when utilized. Indeed, some evidence for this recently has been reported.[16]

Acknowledgements

This work was supported, in part, by the U.S. Air Force Office of Scientific Research, Grant F4962083K0009, Dr. James McMichael, project manager. The technical assistance of W. Bank, R. Meinzer, M. Elwood and K. Jordahl is appreciated.

References

1. Moore, M. and Frei, D., "X-29 and Forward Swept Wing Aerodynamic Overviews." AIAA - 83-1834, AIAA Applied Aerodynamics Conference, Danvers, Massachusetts, July, 1983.

2. Uhad, G.D., Weeks, J.M. and Lange, R., "Wind Tunnel Investigation of Transonic Aerodynamic Characteristics of Forward Swept Wings." J. Aircraft, 20(3) pp 195-202, March, 1983.

3. McCroskey, W.J., "Unsteady Airfoils." Ann. Rev. Fluid Dyn. Annual Reviews, Palo Alto, California: 1982 pp 185-211.

4. McAlister, K.W. and Carr, L.W., "Water Tunnel Visualizations of Dynamic Stall." Journal of Fluids Engineering, Vol. 1D1: pp 376-380, September, 1979.

5. McCroskey, W. J., Carr, L. W. and McAlister, K. W., "Dynamic Stall Experiments on Oscillating Airfoils." AIAA - 75-125, AIAA 13th Aerospace Sciences Meeting, Pasadena, California, January, 1975.

6. Robinson, M.C. and Luttges, M.W., "Unsteady Separated Flow: Forced and Common Vorticity about Oscillating Airfoils." Workshop on Unsteady Separated Flows, Francis, M. and Luttges, M. (eds.), University of Colorado: 1984, pp 117-126.

7. Adler, J. and Luttges, M., "Three-Dimensionality in Unsteady Flow about a Wing." AIAA - 85-0132, AIAA 23rd Aerospace Sciences Meeting, Reno, Nevada, January, 1985.

8. Gad-el-Hak, M. and Ho, C., "Three-Dimensional Effects on a Pitching Lifting Surface." AIAA - 85-0041, AIAA 23rd Aerospace Sciences Meeting, Reno, Nevada, January, 1985.

9. Gad-el-Hak, M., Ho, C. and Blackwelder, R. F., "A Visual Study of a Delta Wing in Steady and Unsteady Motion." Workshop on Unsteady Separated Flows, Francis, M. and Luttges, M. (eds.), University of Colorado: 1984, pp 45-50.

10. Carta, F.O., "Unsteady Stall Penetration of an Oscillating Swept Wing." Workshop on Unsteady Separated Flows, Francis, M. and Luttges, M. (eds.), University of Colorado: 1984, pp 28-37.

11. Ashworth, J., Waltrip, M. and Luttges, M., "Three-Dimensional Unsteady Flow Fields Elicited by a Pitching Forward Swept Wing." AIAA - 86-1104, AIAA 4th Joint Fluid Mechanics, Plasma Dynamics and Lasers Conference, Atlanta, Georgia, May, 1986.

12. Gad-el-Hak, M. and Ho, C., "Unsteady Vortical Flow Around Three-Dimensional Lifting Surfaces." AIAA Journal, Vol. 24, No. 5, pp 713-721, May, 1986.

13. Freymuth, P., Finaish, F. and Bank, W., "Visualization of Wing Tip Vortices in Unsteady and Steady Wind." AIAA - 86-1096, AIAA 4th Joint Fluid Mechanics, Plasma Dynamics and Lasers Conference, Atlanta, Georgia, May, 1986.

14. Robinson, M.C., Gilliam, F., Helin, H., Russell, J. and Walker, J., "Visualization of Three-Dimensional Forced Unsteady Separated Flow." AIAA - 86-1066, AIAA 4th Joint Fluid Mechanics, Plasma Dynamics and Lasers Conference, Atlanta, Georgia, May, 1986.

15. McCormick, Barnes W., Aerodynamics. Aeronautics, and Flight Mechanics, John Wiley and Sons, New York, 1979, pp 61-151.

16. Helin, H.E., and Walker, J.M., "Interrelated Effects of Pitch Rate and Pivot Point on Airfoil Dynamic Stall." AIAA - 85-0130, AIAA 23rd Aerospace Sciences Meeting, Reno, Nevada, January, 1985.